Journal of Materials and Applications 2020;9(1):38-45
https://doi.org/10.32732/jma.2020.9.1.38

# Vanadium Doping Effect on Multifunctionality of $SnO_2$ Nanoparticles

Roman Alvarez-Roca[1], Mariela Desimone[2], Mitchell G. S. da Silva[1], Miguel A. Ponce[2], Elson Longo[1]

*1. CDMF, Department of Chemistry, Federal University of Sao Carlos, Rod. Washington Luiz, Km 235, Sao Carlos – SP CEP 13565-905, Brazil*
*2. INTEMA, Universidad Nacional de Mar de Plata, J. B. Alberdi 2695 (7600), Mar de Plata, Argentina*

Received: 4 April 2020; Accepted: 24 April 2020; Available online:10 May 2020

**Abstract:** In the present study, tin oxide ($SnO_2$) nanoparticles were synthesized by a precursor polymeric method. The obtained nanoparticles were doped with vanadium. The samples were characterized by powder XRD, TEM, optical UV and EPR studies. XRD and TEM showed the rutile crystal structure and its revealed that the lattice cell parameters and particles size were decreased with dopant level. Optical and EPR data confirmed that the doped V enters into $SnO_2$ and distorted the host material symmetry. The films sensing characteristics have been studied from the aspect of doping level of sensing material and microstructure. It is found that V doping on SnO2 enhance sensor sensitivity towards CO gas. The results demonstrated that V doping can improving numerous applications which the $SnO_2$ response is maximized.
**Keywords:** Tin oxide; V-doped; Multifunctional.

## 1. Introduction

These are ceramic materials with multifunctional properties in a single compound applicable for multifunctional activities which are key components nowadays in very diversity technologies under varies conditions [1-3]. These novel multifunctions may be integrated into the materials since have a variety of elements and structures, providing great potential for realizing a diverse range of functions. Thus, two or more kinds of selective properties can be united one another in a cooperative manner. On the other hand, interesting technological applications of nanomaterials are directly related to several factors such as the morphology, size, crystalline phase and activity of a specific surface [2, 4, 5]. Particularity, incorporation of dopant atoms in the pristine crystal structure has a strong influence on the final properties of these materials [4, 6-8]. Additionally, a wide band-gap oxide semiconductor, such as $TiO_2$, $SnO_2$ and ZnO presents several interesting applications. It is observed that when doped with transition metal ions, could showed property remarkable and scientifically puzzling [6-9].

Particularly, $SnO_2$ exhibits chemical, thermal, and mechanical stability with a tetragonal structure of the rutile type. When pure, the oxide is considered an intrinsic semiconductor of type n, having a wide band gap of 3.6 eV and electrical conductivity as a result of the excess of electrons and structural defects. Lattice modifying or forming metals introduced as dopants act as modifying elements of the crystalline and electronic lattice allowing the band gap alteration while aiding in controlling, improving, and creating new properties that can be applied in diverse technological areas, such as sensors [4, 8, 10], varistors [11], solar cells [12], photocatalysts [13, 14], etc. In this work, $SnO_2$ nanoparticles, NPs, with different percentage of vanadium, V (5% and 10%), were successfully prepared by polymeric citrate precursor method. The characterization by X-ray diffraction (XRD), transmission electron microscopy (TEM) and energy-dispersive X-ray spectroscopy (EDS) and UV-vis analyses confirmed that the nanoparticles size and V ions incorporation into the $SnO_2$. The effect of the V doping on optical and magnetic behavior were observed. Finally, electrical and gas sensing behaviors were studied against CO gas under V doping effects.

## 2. Experimental methods

1) Preparation of V-$SnO_2$ samples

The V-$SnO_2$ system was prepared using the polymeric precursor method. Initially, the polymeric precursors of each metal were prepared and then these are mixed to obtain the materials in the desired V dopant concentrations. The following scheme shows the preparation flow chart.

2) V-$SnO_2$ powder characterization

The samples are structurally characterized by X-ray Diffraction (XRD) patterns using a Rigaku D/Max-2000PC diffractometer with Cu Ka radiation. The shape and particle size study carried out by transmission electron microscopy (TEM) operates at 200 kV. This technique will also analyze the elemental composition of the samples by X-ray dispersive energy spectroscopy (EDS). EPR analyses were performed on a Bruker EMX spectrometer (Band X) at room temperature, operating in X band (9 GHz).

3) Electrical and Sensing characterization of V-$SnO_2$ films

The sensor films were obtained by screen printing (from a paste of powders with glycerol) on alumina substrate. Procedures for evaporate water and organics elimination and to improve the films adhesion to substrate were done in an oven at low heating/cooling rate allowing them heating/cooling slowly to avoid cracking on the films. DC-type electric measurements at steady state and no changes in resistance over time were done using the two-wire mode in an Agilent 3440A multimeter. Three different atmospheres (air, vacuum and CO) in a closed chamber and controlled flux were used for gas sensing analysis.

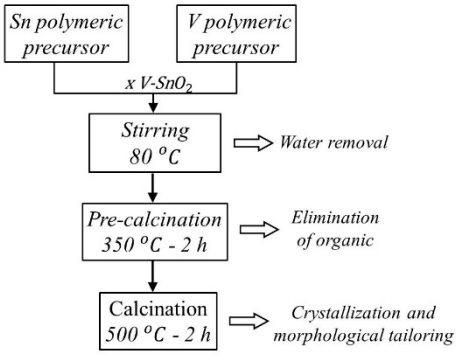


**Scheme 1.** Fluxogram of pure and V-$SnO_2$ nanopowder preparation and processing.

## 3. Results and discussion

### 3.1 Structural and microstructural characterization

The corresponding peaks of tetragonal rutile phase (card JCPDS 21-1250) were identified on the V-$SnO_2$ system at different V contents for XRD measurements as is shown in figure 1. No secondary phases are detected. The lattice parameter and cell volume of the different samples are listed in Table 1. The V introduction into the $SnO_2$ lattice reduce the cell volume, due to $V^{n+}$ incorporation in $Sn^{4+}$ sites (0.68 Å) which decreased lattice spacing due to smaller radius of $V^{3+}$ (0.64 Å), $V^{4+}$ (0.58 Å) or $V^{5+}$ (0.54 Å) ions. Diffraction lines were broadened indicating the nanosized crystallites in all samples; the V-doped samples showed the greatest broadening.

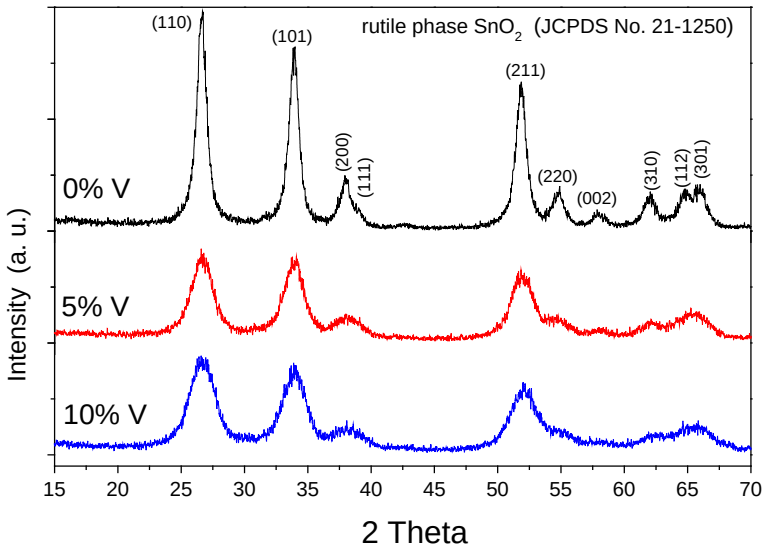


Figure 1. The XRD measurements for V-$SnO_2$ at different V contents.

The crystallite sizes are estimated by Scherrer formula at (110) peak. It is observed in Table 1 that the crystallite size of $SnO_2$ NPs is reduced as a result of increase in V content, this suggests that the V ions prevented the crystal grains growth. Compared with the pure, the intensity of V-doped diffraction peaks decreases sharply, indicating that the doping degrades the $SnO_2$ crystallinity too. Decreased in crystallite size with increasing dopant content also was reported by several works [14-17].

The shape and particle size analysis, examined by TEM micrographia in figure 2 a-c, showed the formation of quasi-faceted NPs in all samples. Their sizes vary in a narrow range around the values previously determined by XRD. In addition, a highly agglomerated degree, as typical for very-fine NPs, was detected on the V-$SnO_2$.

Energy dispersive X-ray spectral analysis (EDS), used for investigating the chemical composition of samples, ensure the presence of Sn and O ions in the host lattice, as seen figure 2d, for all samples and evidently proved that the V ions have been successfully incorporated into the $SnO_2$ host lattice for the doped samples. This size reduction, shown by XRD and TEM, due to V doping enhances the specific surface area to volume ratio, which is a desired requirement for catalytic, sensoring, between other applications.

**Table 1.** Lattice parameter (LP), cell volume, crystallite size, sensitivity, atomic level of the elements and band gab energy of different doped SnO2 nanoparticles.

| V (%) | LP (Å) | | Cell volume | Crystallite size | Atomic % | | | $E_{gb}$ |
|---|---|---|---|---|---|---|---|---|
| | a | c | ($Å^3$) | (nm)* | O | Sn | V | (eV) |
| **0** | 4.733 | 3.180 | 71.24 | 9.07 | 63.5 | 36.5 | - | 3.30 |
| **5** | 4.715 | 3.185 | 70.81 | 4.04 | 55.0 | 40.5 | 4.5 | 2.61 |
| **10** | 4.703 | 3.186 | 70.47 | 3.26 | 64.55 | 28.5 | 6.95 | 2.42 |

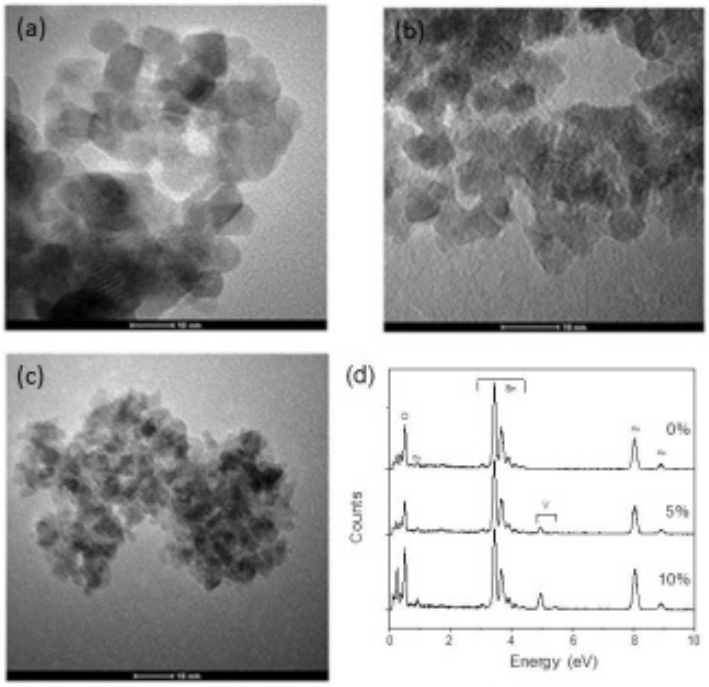


**Figure 2.** TEM images of $SnO_2$ nanoparticles with: (a) 0%, (b) 5% and (c) 10 % of V doping; and (d) EDS spectrums of each V-$SnO_2$ samples.

## 3.2 Optical and magnetical behavior

To have a better understanding of the V effect on optical properties of $SnO_2$, UV-vis spectroscopy is performed. The UV-vis spectrum at reflectance measurements were used to estimate band gap optical energy, $E_{bg}$, considering a direct transition via Kubelka-Munk equation, where $[F(R)\ h\upsilon]^2$ is plotted against incident photon energy, $h\upsilon$, and the extrapolated line at $[F(R)\ h\upsilon]^2 = 0$ gives the $E_{bg}$ in eV as shown in Fig. 3. The values of $E_{bg}$ are listed in Table 1. A significant contribution of V doping on the reduction of the $SnO_2$ band gap value is observed in the figure. The decrease of band gap for the V doping can be caused by the overlapping of 3d and 2p orbital of vanadium and oxygen; those overlapping could initiate the formation of intermediate bands. These $E_{bg}$ values are quite similar or smaller than the reported values for the V-$SnO_2$ system [18, 19].

In order to investigate the magnetism in connection whit electronic configuration of V-$SnO_2$ samples, the EPR experiments were performed. The magnetism behavior could be induced by defects, such as oxygen vacancies,

$V_O$, attributed to the exchange coupling of the spins of electrons trapped in $V_O$. In the present study, an evidence of this $V_O$ magnetic contribution can be observed in undoped $SnO_2$ sample with the $V_O$ characteristic EPR line at g~ 1.89 [20, 21] on figure 4a.

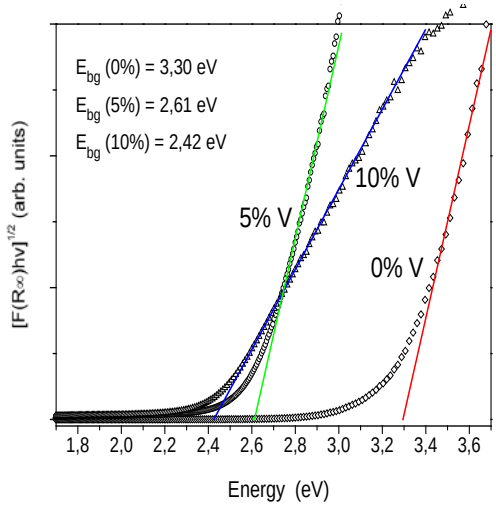


**Figure 3.** UV-visible spectra of pure and V-$SnO_2$ nanoparticles for the band gap energy determination using Tauc approach.

Obviously, the magnetic behavior is enhanced by doping with V ions, the intensity of the EPR signal shows considerable variation with increasing of isolated $V^{n+}$ (n=3, 4 and/or 5). A hyperfine structure with the eight typical components of the unpaired $3d^1$ electron of $^{51}V$ isotope in an axially distorted crystal field [20, 22] is observed for 5 and 10 %. This spectrum is shown only for 5% on figure 4b. The signal intensity for 10% shows a light decreasing compared to 5% and may be due to the formation of $V^{n+}$-$V^{n+}$ clusters, which results from the aggregation because of the more number of V ions.

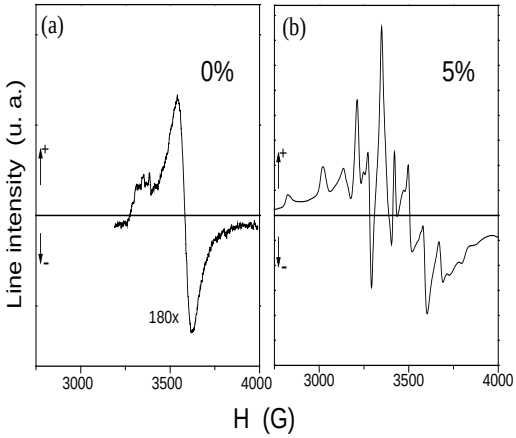


**Figure 4.** Comparative EPR spectrum of pure $SnO_2$ and 5% V doped $SnO_2$ at room temperature.

The V doping improved visible range optical absorption and a clear magnetic improved behavior is associated to the incorporation of V ions into the host system. The present V-$SnO_2$ system could be modified with tailored optical and magnetic properties for functional applications such as magneto-optics and optoelectronic devices.

### 3.3 Electrical and sensing characterization

Electrical conductivity was analyzed from the conductance–temperature characteristics of V-$SnO_2$ samples performed in the three atmospheric conditions: dry air, vacuum and CO gas; at the temperature range of 70 $^oC$ to 500 $^oC$. This conductance, G, variation as a function of inverse of temperature for 5 and 10 % V doped $SnO_2$ sample for each atmosphere is displayed in the figure 5. The temperature dependence of conductance (or conductivity) in this representation is resulting from the known Arrenhuis expression: $G(T) = G_0 \exp(-E_A/kT)$; where $E_A$ is the activation energy for transport process, $G_0$ is a constant of proportionality and k is the Boltzmann constant. The $E_A$ has been calculated from slope of the straight-line plot of logarithmic G vs. temperature inverse.

The $E_A$ values are found to be 0.27, 0.27 and 0.24 eV for air, vacuum and CO atmosphere, respectively, at 5% V-doped $SnO_2$; and 0.27, 0.22 and 0.22 eV for air, vacuum and CO, respectively, at 10 %. These values are expressively lower than the intrinsic $E_A$ for electron transfer from valence band to conduction band on $SnO_2$ (around 3.6 eV). Hence, by the $E_A$ values obtained in the present study, the conduction can be due to thermally excited free electronic carriers from defects/traps at shallow levels transferred to the conduction band. [20, 23, 24]

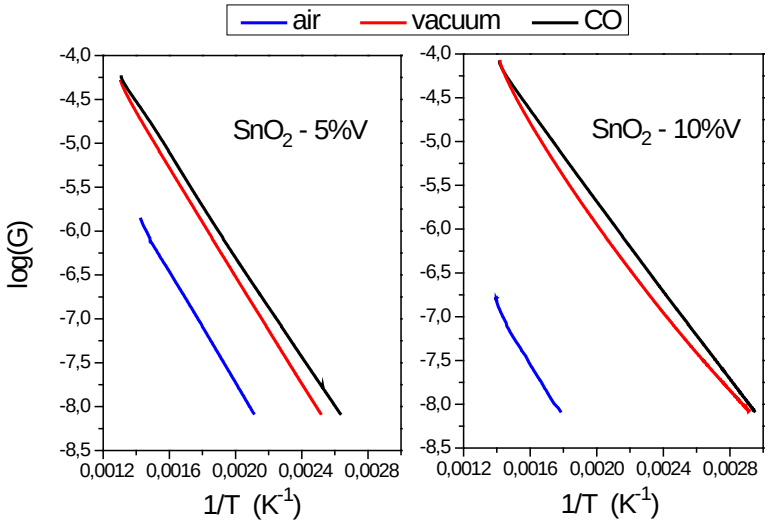


**Figure 5**. Variation of the conductance logarithm as function of 1/T for 5 % and 10% of V doped $SnO_2$ samples at different atmospheres.

For air atmosphere, it can be seen from graph that while the $E_A$ is invariant, the conductance decrease (resistivity increases) with doping concentration which is due to crystallite size reduction from 5 to 10 % previously identified from XRD. As crystallite size decreases, there would be large number of insulating grain boundaries which will hinder the motion of charge carriers thereby increasing the sample resistivity. In contrast, for vacuum and CO atmosphere, a contrary behavior is observed with doping increase. The conductance is increased in correspondence with the $E_A$ reduction. When the $SnO_2$ sensor is kept under the reducing gases (such as CO) the molecules adsorbed can react with surface-oxygen ions ($O^-$, $O_2^-$, $O^{2-}$), leaving electrons and, therefore, leading to higher conductivity (or resistance decrease) as shown in figure 5 for CO atmosphere. A similar process can happen for vacuum. The sensing properties of V-$SnO_2$ films were tested for CO gas from vacuum atmosphere. The vacuum was used initially to clear out films surface and the chamber system. Between the important factors to be considered in designing of gas sensors is the gas sensitivity which is defined as: $S = R_{CO}/R_{vac}$, where $R_{CO}$ and $R_{vac}$ are the samples resistance in presence of CO gas and vacuum atmosphere respectively. The temperature-dependent sensitivity of V doped $SnO_2$ films for CO sensing was studied in the temperature range of 200–500 °C. This behavior is represented in figure 6 for V doped $SnO_2$ films.

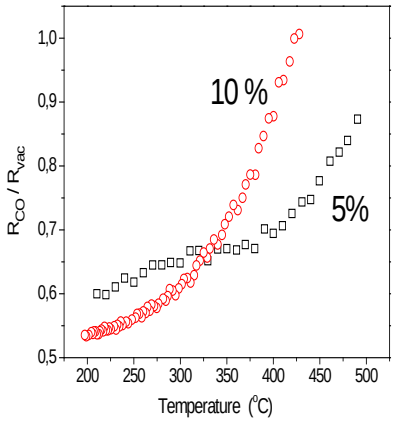


**Figure 6.** Sensitivity at various operating temperatures for V-$SnO_2$ system.

The sensitivity increases with temperature due to sufficient thermal energy essential to overcome the activation energy barrier to active the kinetics of the CO adsorption (surface chemisorption) and surface reaction of the CO molecules adsorbed on sensor surface, leading to the alteration of total resistance of the material. Interestingly, a cross over in sensitivity behavior between 5% and 10 % V doped $SnO_2$ samples can be observed at ~330 $^0$C, which could indicate that the kinetics of the CO chemisorption and reaction on the surface can be dopant concentration dependent. It is clearly seen from figure that the sensitivity increased more suddenly for V doping at 10 %. This concentration dependence could be ascribed as an itself catalytic process activates with the V increasing.

The response magnitude (or sensor response) and response time are another important factors to be considered in gas sensors performance. The response magnitude, RM, is defined as the ratio of total change in the resistivity, from an initial reference value (baseline), generally the $R_{vac}$ value at moment of gas input, between current $R_{CO}$ to the initial reference value in vacuum; here: $RM=((R_{vac}-R_{CO})/R_{vac})x100\%$. Response time is defined as the time period required for the resistance to reach 90% of the total change value when exposed to CO gas, here the response time is identified as $t_{90}$. The RM and response time of V-$SnO_2$ sensor were tested for two different CO concentrations, 70 and 140 ppm, at 300 $^0$C. To compare the effect of doping amount on the RM, samples with different V doping were compared for their RM values at $t_{90}$. Figure 7 shows the RM of both doping level (5 and 10 %) at 300°C for two different CO concentrations. The 10 %V-doping based sensor is favorably higher (60 %) than the 5% based one (47%) in lower CO gas concentration (70 ppm). To the contrary, in high concentration range (140 ppm), 5% based sensor offered superior RM (62%) in comparison with the 10% based one (43%).

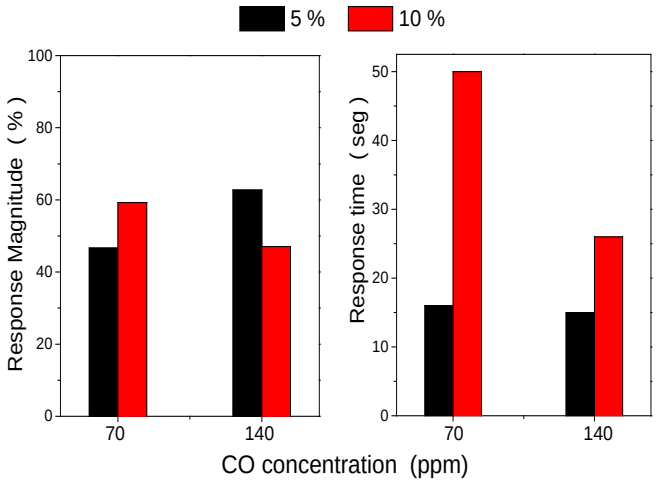


**Figure 7.** Variation of response magnitude and response time for V-$SnO_2$ sensor for two different CO concentrations at the operating temperature of 300 $^o$C.

However, the 5% base sensor showed faster response (lower $t_{90}$) than that of 10 % one, as shown too in figure 7, for both CO concentrations. Moreover, at lower CO concentrations the difference in $t_{90}$ (between 5 and 10 %) is significantly higher compared to that in the higher gas concentration. It could be envisaged from size behavior that a better sensor performance (higher RM and lower $t_{90}$) for the 10 % base sensor (with lower particles size) possibly attributed to its better surface to volume ratio. But this behavior is not rigorously observed, and future analyzes should be made considering doping effects on other factors such as: chemisorption mechanisms, types of defects, etc. Thus, variations of the dopant concentration allow significant tuning of electrical and sensing behavior, with respect to transport mechanism, sensor sensitivity, response sensor, and other sensor's parameters. This electrical and sensoring behavior of the V-$SnO_2$ nanosystem can be used as electronic devices, CO chemical sensors, biosensors, between others with very high sensitivity, selectivity, and stability.

## 4. Conclusions

The pure and vanadium doped $SnO_2$ nanoparticles were synthesized by a simple polymeric precursor process. The influence of the doping degree on structure crystal and microstructure, by XRD and TEM, respectively of these nanoparticles was investigated. The XRD measurements and TEM analysis show a decrease of the unit cell volume and particles size of the doped sample as compared with the undoped $SnO_2$. This behavior established that the V ions are successfully incorporated into the $SnO_2$ lattice by the Sn ions substitution. Based on the modifications observed on the optical analysis, EPR spectra, and electrical and sensing measurements it has been sustained similar conclusion: the V ion species are incorporated into the $SnO_2$ with improvements on several of

these behaviors. Because of these interesting modifications by doping, this system could be useful for optoelectronic and magneto-optic devices, environmental remediation by photocatalytic processes and for gas control.

## 5. References


[1] Salonitis K, Pandremenos J, Paralikas J, Chryssolouris G. Multifunctional materials: engineering applications and processing challenges. The International Journal of Advanced Manufacturing Technology. 2010;49:803-826.

[2] Ferreira AD, Novoa PR, Marques AT. Multifunctional material systems: A state-of-the-art review. Composite Structures. 2016;151:3-35.

[3] Calais T, Alvarado PV. Advanced functional materials for soft robotics: Tuning physicochemical properties beyond rigidity control. Multifunctional Materials. 2019;2:042001.

[4] Sun YF, Liu SB, Meng FL, Liu JY, Jin Z, Kong LT, Liu JH. Metal oxide nanostructures and their gas sensing properties: A review. Sensors. 2012;12(3):2610-2631.

[5] Thong LV, Loan LTN, Hieu NV. Comparative study of gas sensor performance of $SnO_2$ nanowires and their hierarchical nanostructures. Sensors and Actuators B: Chemical. 2010;150(1):112-119.

[6] Rahimi N, Pax RA, Gray EM. Review of functional titanium oxides. I: TiO2 and its modifications. Progress in Solid State Chemistry. 2016;44(3):86-105.

[7] Gupta P, Rathore V. A comprehensive review: SnO2 for photovoltaic and gas sensor applications. Applied Innovative Research. 2019;1:184-193.

[8] Garshev AV, Ivanov VK, Krotova AA, Filatova DG, Konstantinova EA, Naberezhnyi DO, Khmelevsky NO, Marikutsa AV, Kots PA, Smirnov AV, Rumyantseva MN. Enhancement of Lewis acidity of Cr-Doped nanocrystalline $SnO_2$: Effect on surface $NH_3$ oxidation and sensory detection pattern. ChemPhysChem. 2019;20(15):1985-1996.

[9] Zhou H, Li Z, Niu X, Xia X, Wei Q. The enhanced gas-sensing and photocatalytic performance of hollow and hollow core–shell $SnO_2$-based nanofibers induced by the Kirkendall effect. Ceramics International. 2016;42(1):1817-1826.

[10] Wang CT, Chen MT. Vanadium-promoted tin oxide semiconductor carbon monoxide gas sensors. Sensors and Actuators B: Chemical. 2010;150(1):360-366.

[11] Lustosa GM, da Costa JP, Perazolli LA, Stojanovic BD, Zaghete MA. Electrophoretic deposition of (Zn, Nb) $SnO_2$-films varistor superficially modified with $Cr^{3+}$. Journal of the European Ceramic Society. 2015;35(7):2083-2089.

[12] Batmunkh M, Dadkhah M, Shearer CJ, Biggs MJ, Shapter JG. Incorporation of graphene into $SnO_2$ photoanodes for dye-sensitized solar cells. Applied Surface Science. 2016;387:690-697.

[13] Reddy CV, Babu B, Vattikuti SP, Ravikumar RV, Shim J. Structural and optical properties of vanadium doped $SnO_2$ nanoparticles with high photocatalytic activities. Journal of Luminescence. 2016;179:26-34.

[14] Letifi H, Litaiem Y, Dridi D, Ammar S, Chtourou R. Enhanced photocatalytic activity of vanadium-doped $sno_2$ nanoparticles in rhodamine B degradation. Advances in Condensed Matter Physics. 2019;2019:2157428.

[15] Sabri NS, Deni MS, Zakaria A, Talari MK. Effect of Mn doping on structural and optical properties of $SnO_2$ nanoparticles prepared by mechanochemical processing. Physics Procedia. 2012;25:233-239.

[16] Pascariu P, Airinei A, Grigoras M, Fifere N, Sacarescu L, Lupu N, Stoleriu L. Structural, optical and magnetic properties of Ni doped $SnO_2$ nanoparticles. Journal of Alloys and Compounds. 2016;668:65-72.

[17] Kumar V, Singh K, Jain M, Kumar A, Sharma J, Vij A, Thakur A. Role of Cu in engineering the optical properties of $SnO_2$ nanostructures: Structural, morphological and spectroscopic studies. Applied Surface Science. 2018;444:552-558.

[18] Soltan WB, Mbarki M, Ammar S, Babot O, Toupance T. Structural and optical properties of vanadium doped $SnO_2$ nanoparticles synthesized by the polyol method. Optical Materials. 2016;54:139-146.

[19] Shyamala R, Devi LG. Synthesis, characterisation and evaluation of photocatalytic activity of V-doped $SnO_2$ semiconducting particles under solar light. REST Journal on Emerging Trends in Modelling and Manufacturing. 2018;4(1):16-22.

[20] Ningthoujam RS, Lahiri D, Sudarsan V, Poswal HK, Kulshreshtha SK, Sharma SM, Bhushan B, Sastry MD. Nature of $V^{n+}$ ions in $SnO_2$: EPR and photoluminescence studies. Materials Research Bulletin. 2007;42(7):1293-1300.

[21] Toloman D, Popa A, Raita O, Stan M, Suciu R, Miclaus MO, Biris AR. Luminescent properties of vanadium-doped $SnO_2$ nanoparticles. Optical Materials. 2014;37:223-228.

[22] Popa A, Toloman D, Raita O, Stan M, Pana O, Silipas TD, Giurgiu LM. Ferromagnetic behaviour of vanadium doped $SnO_2$ nanoparticles annealed at different temperatures. Journal of Alloys and Compounds. 2014;591:201-206.

[23] Joseph DP, Renugambal P, Saravanan M, Raja SP, Venkateswaran C. Effect of Li doping on the structural, optical and electrical properties of spray deposited $SnO_2$ thin films. Thin Solid Films. 2009;517(21):6129-6136.
[24] Benouis CE, Benhaliliba M, Yakuphanoglu F, Silver AT, Aida MS, Juarez AS. Physical properties of ultrasonic sprayed nanosized indium doped $SnO_2$ films. Synthetic Metals. 2011;161:1509-1516.